Testing system for ferromagnetic shape memory microactuators

Y. Ganor, D. Shilo, J. Messier, T. W. Shield, and R. D. James

Citation: Review of Scientific Instruments **78**, 073907 (2007); doi: 10.1063/1.2753672
View online: http://dx.doi.org/10.1063/1.2753672
View Table of Contents: http://scitation.aip.org/content/aip/journal/rsi/78/7?ver=pdfcov
Published by the AIP Publishing

Articles you may be interested in

Frequency response of acoustic-assisted Ni–Mn–Ga ferromagnetic-shape-memory-alloy actuator
J. Appl. Phys. **105**, 093923 (2009); 10.1063/1.3125307

Magnetization dependence on dynamic strain in ferromagnetic shape memory Ni–Mn–Ga
Appl. Phys. Lett. **93**, 062501 (2008); 10.1063/1.2969799

Reduction in required magnetic field to induce twin-boundary motion in ferromagnetic shape memory alloys
J. Appl. Phys. **95**, 6965 (2004); 10.1063/1.1687292

Magnetomechanical testing machine for ferromagnetic shape-memory alloys
Rev. Sci. Instrum. **74**, 4077 (2003); 10.1063/1.1599072

Model for discontinuous actuation of ferromagnetic shape memory alloy under stress
J. Appl. Phys. **89**, 1295 (2001); 10.1063/1.1285867

AIP Journal of Applied Physics

Journal of Applied Physics is pleased to announce André Anders as its new Editor-in-Chief

This article is copyrighted as indicated in the article. Reuse of AIP content is subject to the terms at: http://scitationnew.aip.org/termsconditions. Downloaded to IP: 128.101.142.152 On: Wed, 13 Aug 2014 18:46:48

Testing system for ferromagnetic shape memory microactuators

Y. Ganor[a] and D. Shilo
Department of Mechanical Engineering, Israel Institute of Technology-Technion, Haifa 32000, Israel

J. Messier, T. W. Shield, and R. D. James
Department of Aerospace Engineering and Mechanics, University of Minnesota, Minneapolis, Minnesota 55455

(Received 10 May 2007; accepted 26 May 2007; published online 23 July 2007)

Ferromagnetic shape memory alloys are a class of smart materials that exhibit a unique combination of large strains and fast response when exposed to magnetic field. Accordingly, these materials have significant potential in motion generation applications such as microactuators and sensors. This article presents a novel experimental system that measures the dynamic magnetomechanical behavior of microscale ferromagnetic shape memory specimens. The system is comprised of an alternating magnetic field generator (AMFG) and a mechanical loading and sensing system. The AMFG generates a dynamic magnetic field that periodically alternates between two orthogonal directions to facilitate martensitic variant switching and to remotely achieve a full magnetic actuation cycle, without the need of mechanical resetting mechanisms. Moreover, the AMFG is designed to produce a magnetic field that inhibits 180° magnetization domain switching, which causes energy loss without strain generation. The mechanical loading and sensing system maintains a constant mechanical load on the measured specimen by means of a cantilever beam, while the displacement is optically monitored with a resolution of approximately 0.1 μm. Preliminary measurements using Ni_2MnGa single crystal specimens, with a cross section of 100×100 μm^2, verified their large actuation strains and established their potential to become a material of great importance in microactuation technology. © *2007 American Institute of Physics.*
[DOI: 10.1063/1.2753672]

I. INTRODUCTION

Materials that alter their properties in response to physical changes are classified as active materials. These materials are commonly applied as actuation devices in microelectromechanical systems. Many of these systems require large strokes (displacements) by a small component, which means large actuation strains. However, most active materials are either limited to very small strains, as piezoelectric and magnetostrictive materials, or to a slow response, as shape memory alloys. In recent years, a new class of active materials known as ferromagnetic shape memory (FSM) alloys has received much attention due its large reversible strains when exposed to magnetic fields.[1–3] So far, reversible strains of up to about 6% have been observed in tetragonal phase of Ni_2MnGa FSM single crystals[4–6] and 10% in the orthorhombic phase.[7] This is at least an order of magnitude larger than other so-called giant magnetostrictive materials such as Terfenol-D.[8] The unique combination of large strains and fast response[9–11] makes these materials promising for a variety of applications. Potential applications include devices for micropump systems, vibration and signature control, novel aerodynamic and hydrodynamic control systems, active shock systems, and sonar devices.[12–16]

Ferromagnetic shape memory alloys are both ferromagnetic and capable of undergoing a structural phase transformation.[1] Unlike conventional shape memory alloys, which can only be actuated by changing their temperature, these materials can be actuated also by magnetic fields. The FSM effect refers to either the reversible field-induced austenite to martensite transformation or the field-induced martensitic variant switching leading to an overall change of shape. Theoretically, it is possible to field induce a phase transformation but this effect necessitates extremely large fields in the known FSM materials, while martensitic variant switching can be induced by reasonable magnetic fields. Because magnetic fields are much easier and faster to apply remotely to a material, FSM alloys have significant advantage over conventional shape memory materials.[2] When a FSM single crystal is cooled from the austenitic phase to below the phase transformation temperature, a martensitic variant microstructure develops with complex twinned variant structure, unless it has been biased with a stress or a magnetic field toward one particular variant. The presence of variant microstructure and field-induced variant switching allows for processes which can lower the total energy of the material. Experimental results[4] indicate that the application of fields in the martensitic state can produce a variety of processes such as magnetic domain wall motion, variant nucleation, twin-boundary motion, and magnetization rotation. The driving energies for these processes are in general different and all compete to reduce the total energy of the system. In high magnetocrystalline anisotropy materials such as Ni_2MnGa, variant nucleation and variant switching offer more efficient energy

[a]Electronic mail: yanivg@tx.technion.ac.il

 © 2007 American Institute of Physics

This article is copyrighted as indicated in the article. Reuse of AIP content is subject to the terms at: http://scitationnew.aip.org/termsconditions. Downloaded to IP: 128.101.142.152 On: Wed, 13 Aug 2014 18:46:48

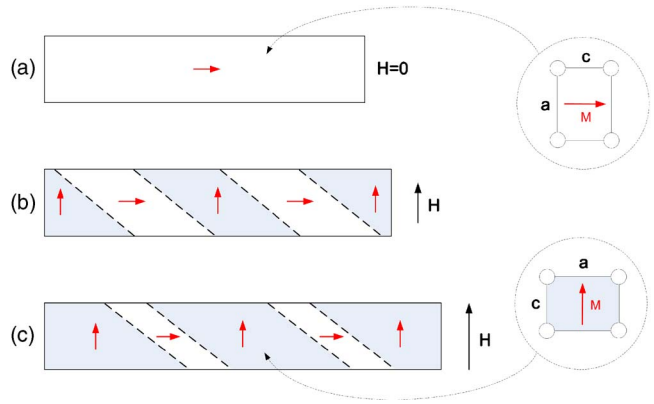

FIG. 1. (Color online) A schematic presentation of the magnetomechanical effect in Ni_2MnGa single crystal. The black dashed lines show the twin boundaries in the deformed tetragonal lattice. The regions between the twin boundaries represent different variants. When an increasing magnetic field is applied, the twin boundaries move to increase the volume fraction of the favorably aligned variant, which results in an overall strain of the specimen.

mechanisms for reducing the system's free energy than magnetization rotation, and therefore the switching effect may be energetically preferred.

The basic phase transformation in Ni_2MnGa is from cubic unit cell to tetragonal unit cell, which occurs when the material is cooled below a characteristic transformation temperature. The transformation temperature can be adjusted by the concentration of the $Ni_2Mn_{(1+x)}Ga_{(1-x)}$ nonstoichiometric alloy. In this transformation a cubic unit cell is contracted along one axis and elongated along the other two. A typical martensitic microstructure consists of mixtures of these three variants in which two adjacent variants meet at well-defined twin boundaries. The austenite phase lattice parameter is $a_0=2.91$ Å and the tetragonal lattice parameters are $a=2.95$ Å and $c=2.77$ Å (in $Ni_{51.3}Mn_{24.0}Ga_{24.7}$).[2] A typical FSM strain related variant switching effect is depicted in Fig. 1. In Fig. 1(a), a specimen of a single variant is illustrated. The c axis of the unit cell is aligned along the long axis of the sample. When an external magnetic field is applied in direction perpendicular to the c axis, as shown in Figs. 1(b) and 1(c), it acts to align the magnetization toward this direction. This change of the magnetization occurs by a martensitic variant rearrangement, which includes an increase of the volume fraction of variants with easy axes in the direction of the applied field. As a result, the length of the sample increases by the amount of the ratio a/c.

Substantial efforts have been directed at understanding the phenomenology and determining the magnetomechanical properties of Ni_2MnGa alloys, and numerous actuation experiments[9,10,17] and commercial devices[12,13] were realized. In these actuators, the FSM elements have typical dimensions in the centimeter scale and are induced by a magnetic field directed along a single axis. In order to return the element into its original shape, a spring mechanism is used to provide a restoring compressive force. Consequently, an application of a dynamic magnetic field which changes along two perpendicular axes offers a novel way to remotely activate the FSM element. A breakthrough in actuation experiments has been recently achieved by an apparatus called a magnetomechanical testing machine.[18] This machine allows mechanical testing of specimens with typical cross section of $100\ \mu m \times 100\ \mu m$ using the application of a dual-dipole electromagnet, limited to variable magnetic field frequencies lower than 1 kHz. However, the magnetomechanical behavior of microscale FSM specimens has not been studied yet. Work continues on improving Ni_2MnGa alloys and as such, the full potential of these materials has yet to be realized. Specifically, several conceptual designs for FSM microactuators based on released single crystal films have been proposed and thin freestanding FSM films have been produced.[15,16]

This article presents a novel experimental system that measures the dynamic magnetomechanical behavior of FSM specimens and is the first to propose studying small-scale FSM devices. Moreover, the FSM elements are remotely activated by a unique alternating magnetic field generator (AMFG), without the need of a mechanical restoring force.

II. EXPERIMENTAL SETUP

A. General description of the apparatus

The apparatus discussed here was designed to apply a combination of variable direction magnetic field of approximately 7.5×10^3 Oe and mechanical loads of up to 10 MPa, for direct measurement of actuation strains caused by magnetically induced variant switching. The specimen displacement has been monitored with a resolution of about 0.1 μm. This was implemented by measuring the angle of a reflected laser beam off the surface of silicon cantilever held against the free surface of the sample. All experiments were performed using single crystal Ni_2MnGa specimens, which were oriented by means of a Laue x-ray diffractometer and cut to dimensions of up to $100\ \mu m \times 100\ \mu m \times 5$ mm by a wire electro discharge machining (EDM) with faces parallel to the [100] directions.

The stress and strain in the specimen were determined by applying the Euler-Bernoulli beam theory to the measured deflection of the cantilever as described below. The magnetomechanical actuation device was comprised of a mechanical device for loading and sensing, magnetic field generator, cooling device, and a video imaging system, as sketched in Fig. 2 and pictured in Fig. 3.

B. Loading and sensing apparatus

The displacement measurement of the FSM alloy specimen is based on the measurement of the deflection of a silicon cantilever, which is in contact with the free end of the specimen, by means of laser beam reflection (Melles Griot®, HeNe 2 mW) using set of polarizers, mirrors, beam splitter, and a wave plate (see Figs. 4–6). The reflection off the surface of the cantilever is collected by a position sensitive detector (PSD) (Duma optronics LTD, Spotana-9), filtered with an analog low-pass filter set at a cutoff frequency of 50 Hz (Cygnus Technology Inc., FLA-01), and recorded with a two channel digital storage oscilloscope (Tektronix, TDS 1012). The optical setup was based on the concept of light polarization rotators to act as an optical gate. The optical gate ensures that the light reflected from the cantilever is read by the

This article is copyrighted as indicated in the article. Reuse of AIP content is subject to the terms at: http://scitationnew.aip.org/termsconditions. Downloaded to IP: 128.101.142.152 On: Wed, 13 Aug 2014 18:46:48

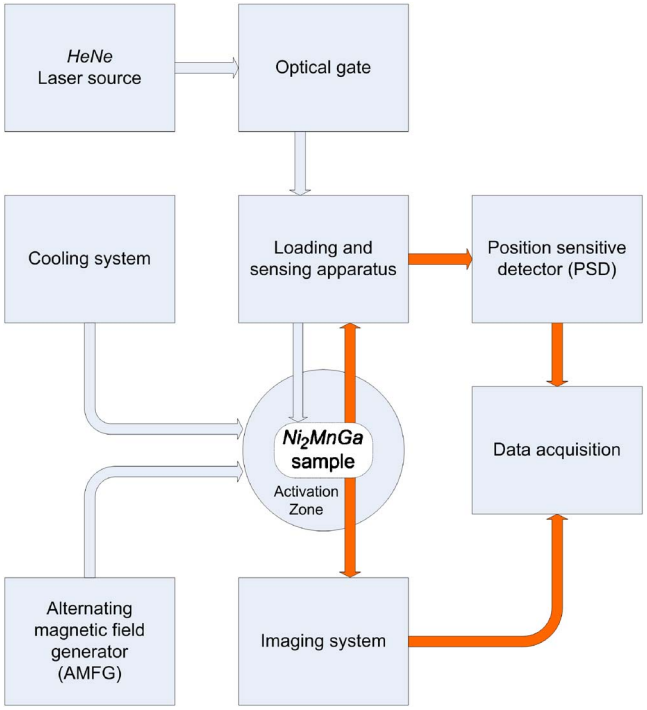

FIG. 2. (Color online) A schematic description of the experimental setup. Blue arrows indicate input sources and red arrows indicate output measurement data. A detailed description of the optical gate is depicted in Fig. 4, the loading and sensing apparatus is depicted in Fig. 5, the cooling system is depicted in Fig. 6, and the AMFG is depicted in Fig. 7.

PSD without secondary reflections from other optical planes or reflection of light back to the laser source. Light traveling in the forward direction is polarized by the beam splitter, and then circularly polarized by a wave plate. Upon reflection from the cantilever, the direction of circular polarization is reversed, so that upon transmission back through the wave plate it becomes polarized in the orthogonal direction and is therefore blocked by the polarizing beam splitter cube from returning to the laser.

The PSD measures the two dimensional (X_{PSD}-Y_{PSD}) position of the light beam that hits its surface. Its resolution is about 1 μm. The output of the PSD is recorded using an oscilloscope and stored for later analysis. The analysis was based on the Euler-Bernoulli beam theory to determine the strain and the applied force on the silicon cantilever. Under the boundary conditions of our setup, the calculated angle of deflection $\theta_c(z_0)$ as a function of the displacement $v(L)$ is

$$\theta_c(z_0) = \frac{3z_0(2L - z_0)}{2L^3} v(L), \tag{1}$$

where z_0 is the refraction point of the laser from the cantilever and L is the total length of the cantilever. From a simple geometric argument, the angle measured by the PSD is twice

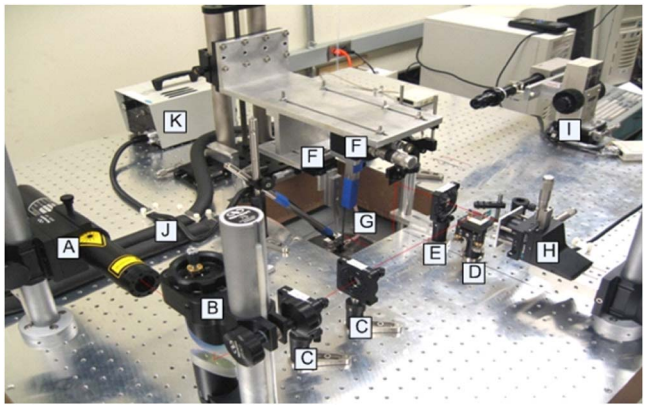

FIG. 3. (Color online) A picture of the entire testing system is shown. The labels are as follows: (A) 2 mW HeNe 632 nm laser, (B) axial telescopic mirrors, (C) linear polarizer, (D) polarizer cubic beam splitter, (E) quarter wave plate, (F) differential flexure microstage, (G) activation zone and the alternating magnetic field generator (AMFG), (H) lateral position sensitive detector, (I) long distance focal microscope, (J) cooling device, and (K) optic fiber light source.

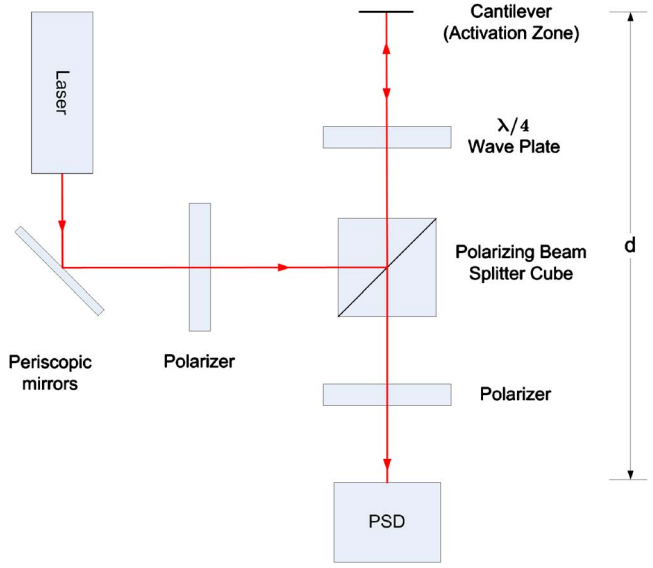

FIG. 4. (Color online) A schematic description of the optical apparatus.

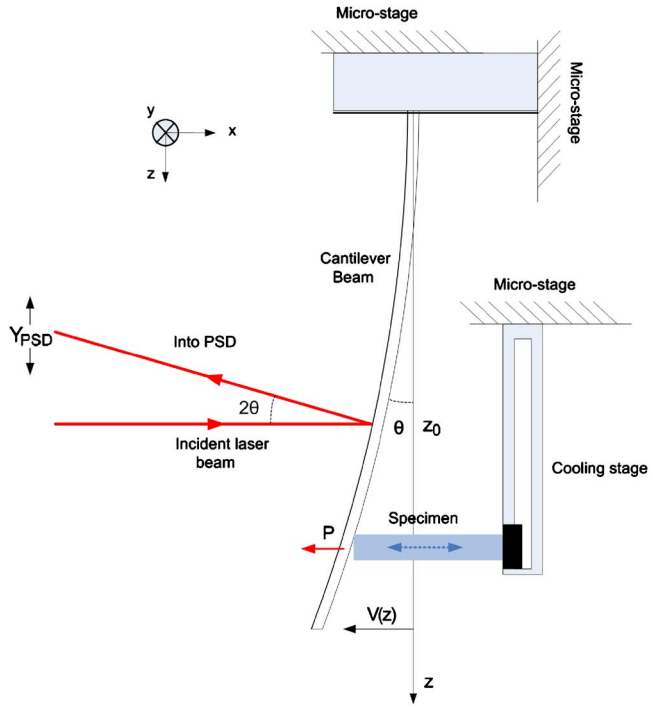

FIG. 5. (Color online) A schematic close-up view of the mechanical loading and sensing apparatus.

This article is copyrighted as indicated in the article. Reuse of AIP content is subject to the terms at: http://scitationnew.aip.org/termsconditions. Downloaded to IP: 128.101.142.152 On: Wed, 13 Aug 2014 18:46:48

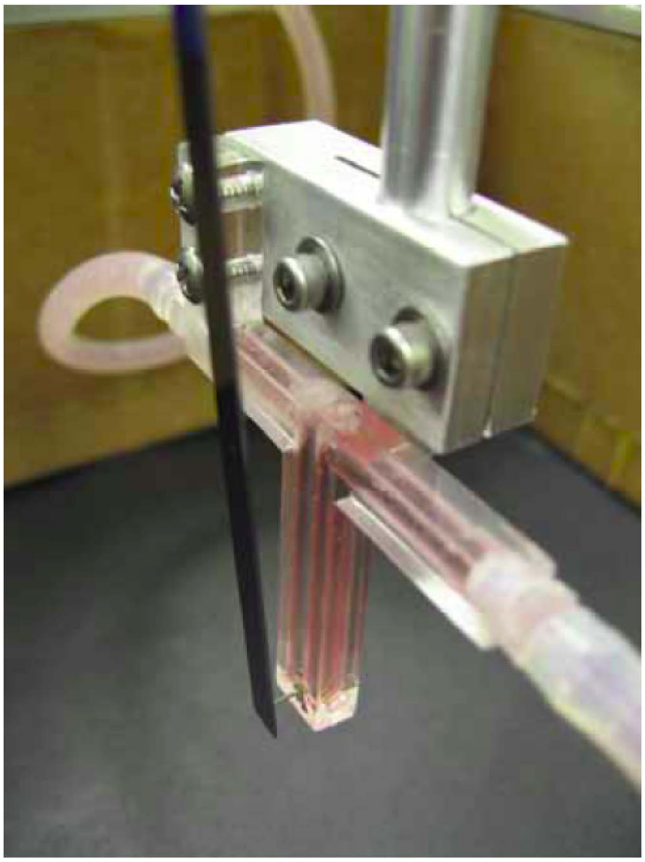

FIG. 6. (Color online) A photograph of the mechanical loading and sensing apparatus.

the angle of deflection of the silicon cantilever. With this taken into account, the measured angle θ_m on the PSD is given by

$$\theta_m = \frac{Y_{\mathrm{PSD}}}{2d}, \tag{2}$$

where Y_{PSD} is the output component of the measured displacement on the PSD along the relevant direction and d is the length of the optical path (Fig. 4). Before the application of the magnetic field, a mechanical load is applied to the specimen by moving the cantilever toward the specimen using a three-axis microstage. The relationship between the cantilever deflection $v(z)$ and the force applied on the specimen P is

$$v(z) = \frac{PL}{EI}\left(\frac{z^2}{2} - \frac{z^3}{6L}\right). \tag{3}$$

The cantilever length is chosen such that its initial deflection is about two orders of magnitude larger than the specimen displacements due to the magnetomechanical effect and hence the force on the specimen is approximately constant during the experiment. Under these conditions, the motion of the specimen induced by the magnetic fields is sensed and measured. To isolate vibrations, a pneumatic isolation table was used to support the specimen and instrumentation. The table consists of a medium density fiberboard (MDF) open box frame, a construction foam core, and aluminum top. MDF was chosen as a frame for its rigidity and lack of electrical conductivity and magnetic properties. The table is supported by four vertical pneumatic isolators (Newport Inc.). The optical components are clamped to the isolation table with highly damped material posts and post holders (Newport Inc.).

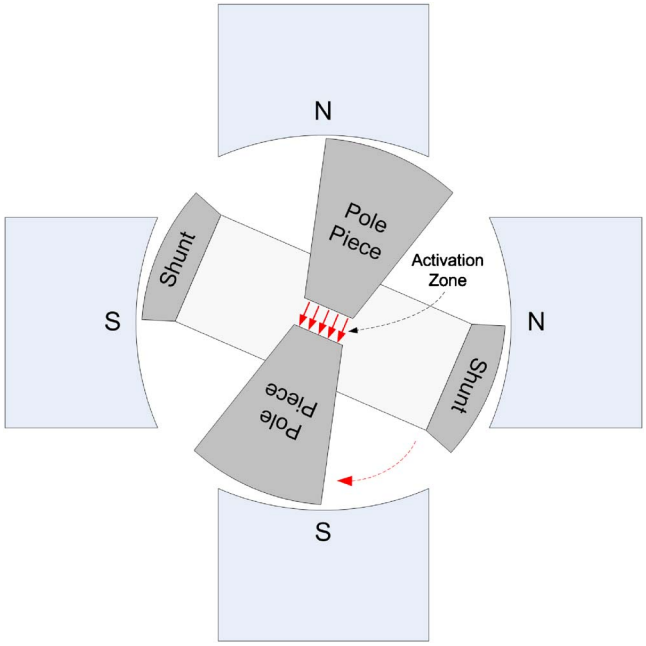

FIG. 7. (Color online) A schematic illustration of the AMFG.

C. Alternating magnetic field generator (AMFG)

The magnetic fields were generated by a unique AMFG which has been especially developed to provide an alternating magnetic field at frequencies of up to 1 kHz (currently it provides up to 70 Hz). The instrument was designed to generate two alternating orthogonal magnetic fields H_1, H_2, as needed for the variant switching experiments. That field structure is important both to minimize nucleation of 180° magnetization domains, which cause energy loss without strain production, and to provide two way actuation. The generator comprises of two perpendicular pairs of permanent magnets and a rotor which contains a pair of pole pieces and a field shunt, as shown in Figs. 7 and 8. When the pole pieces are located between one pair of magnets, they channel the magnetic field to the air gap, referred to as the activation zone. At the same time the shunt prevents the magnetic field of the second pair of magnets from generating magnetic field in the activation zone by providing a magnetic circuit around the activation zone. After a 90° rotation the role of the magnets is swapped, and thus the alternating magnetic field is generated.

D. Cooling device

To ensure that the specimen is at the martensite phase, it has to be held at a steady temperature below the martensite finish temperature. The specimen temperature was controlled by a special designed T-shaped cooling device and temperature controlled bath. The T-shaped cooling device is constructed of Lexan and brass and is designed to connect to a

This article is copyrighted as indicated in the article. Reuse of AIP content is subject to the terms at: http://scitationnew.aip.org/termsconditions. Downloaded to IP: 128.101.142.152 On: Wed, 13 Aug 2014 18:46:48

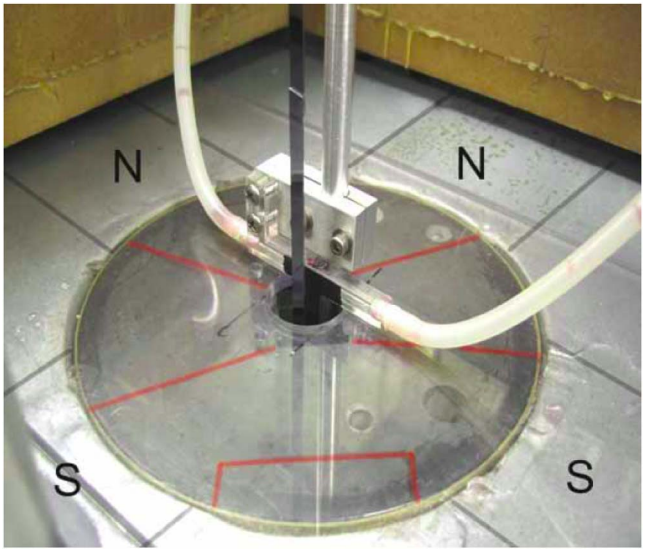

FIG. 8. (Color online) A photograph of the AMFG.

microstage arm (Fig. 6). A closed loop channel runs through the center of the device, through which cooled antifreeze liquid (ethylene glycol, 50%) flows. The fluid flow is provided by the controlled bath (Polyscience Inc., model 9710). The specimen was glued to a brass screw that was in contact with the fluid. The shape of the T holder was designed to suspend the specimen in the center of the AMFG activation zone. The specimens were attached to the T-shaped cooling device with flexible heat-conductive silver epoxy. The T-shape cooling device is then held in the activation zone by an aluminum rod and clamp attached to the same stage as the silicon cantilever. Two triple-axis differential micrometer stages were used to position the flat surface of the cantilever against the tip of the Ni_2MnGa specimen in the activation zone. The microstages allow for very fine control over the applied stress on the specimen.

E. Dry N_2 environment

The martensitic phase temperature for Ni_2MnGa is below the dew point and therefore condensation may form on its surface. To overcome this effect, a dry nitrogen container was placed around the T-shaped cooling device during operation. The dry nitrogen container is a large piece of plastic wrap, draped around the cooling device and taped to the surface of the isolating table. The evaporation of condensation on the surface was monitored with a microscope.

F. Imaging video system

Observation of phase transitions and variant switching requires the use of high power optics. For these purposes we have developed a setup comprised of a microscope (Optem Zoom 70) in conjunction with an assortment of lenses, an optic fiber white light source, and a video camera. Images of the surface of the specimen were acquired and recorded to a video tape.

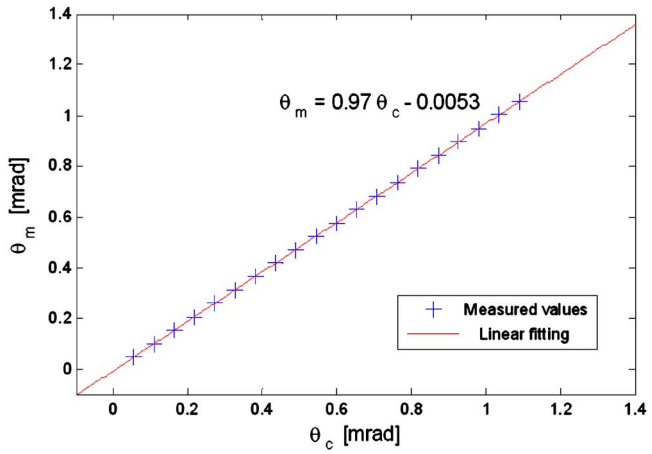

FIG. 9. (Color online) Measured vs calculated angle of deflection.

III. CALIBRATION AND SYSTEM CAPABILITIES

To validate the performance of the force application and displacement sensing apparatus, a preliminary experiment has been performed. The purpose of this experiment was to test the capability of applying deflection (i.e., force) on a cantilever by means of a nanopositioning stage motor (PI Inc.) and measuring the deflection with a sufficient accuracy by means of the optical apparatus. An alignment and calibration procedure of the optical setup components was performed to get a match between the theoretical beam deflection (1) and the values measured by the PSD (2). The results show an excellent fit between the angle calculated from the displacement applied by the nanopositioner and the angles measured by the PSD (see Fig. 9).

The strain measurement capability of the setup is limited by its displacement resolution. The deflection of the cantilever is equal to the displacement of the specimen, u_S. Because $u_S \ll L$ and $Y_{\mathrm{PSD}} \ll d$, the measured angle of the beam deflection θ_m by the small angle approximation is

$$\theta_m = \frac{Y_{\mathrm{PSD}}}{2d} \approx \frac{u_S}{L}. \tag{4}$$

Therefore, the displacement resolution is

$$\Delta u_S \approx \frac{L}{2d} \Delta Y_{\mathrm{PSD}}. \tag{5}$$

The PSD resolution is $\Delta Y_{\mathrm{PSD}} = 1\ \mu$m, and for cantilever length of $L = 15$ cm, $d = 50$ cm, we get a displacement resolution of approximately $\Delta u_S = 150$ nm. This value gives a strain resolution of 3×10^{-5} for a specimen length of 5 mm. For microscale specimens of typical length of 500 μm, the strain resolution is 3×10^{-4}, which is still two orders of magnitude better than the expected magnetomechanical actuation strains. The force measurement resolution capability of the setup [derived from Eq. (3)] is

$$\Delta P = \frac{EI}{dL^2} \Delta Y_{\mathrm{PSD}}. \tag{6}$$

For a rectangular beam $I = bh^3/12$, where b and h are the width and height, respectively. A substitution of $\Delta Y_{\mathrm{PSD}} \approx 1\ \mu$m, $E = 140$ GPa, $b = 5$ mm, $h = 0.5$ mm, and

This article is copyrighted as indicated in the article. Reuse of AIP content is subject to the terms at: http://scitationnew.aip.org/termsconditions. Downloaded to IP: 128.101.142.152 On: Wed, 13 Aug 2014 18:46:48

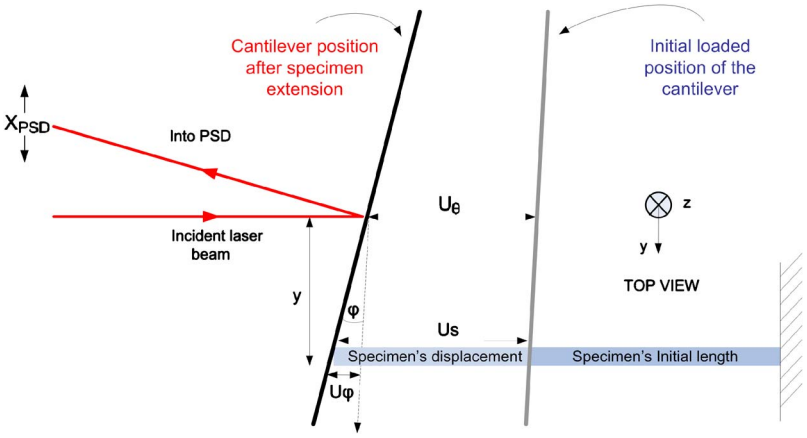

FIG. 10. (Color online) A top-view illustration of the contact point between the cantilever beam and specimen. The deviation y of the contact point from the cantilever median is significantly exaggerated.

$L=15$ cm in Eq. (6) yields $\Delta P \approx 0.65$ μN. This value gives a stress resolution of 1.6×10^{-5} MPa for a specimen cross section of 200×200 μm^2. For reduced cross sections of 50×1 μm^2, the stress resolution still holds a reasonable value of 10^{-2} MPa. Therefore, the force/displacement resolutions demonstrate the capabilities of the apparatus to study FSM microspecimens based on thin freestanding films.

To account for the point of contact between the specimen and the cantilever beam off center, consider the geometry shown in Fig. 10 (not to scale). In this figure, a top view of the sample and of the cantilever is depicted at its initial loaded position and of its final position after the sample's displacement. We denote the contact point distance from the center line of the cantilever as y, the sample's displacement u_s, the angle of twist φ, and the bending (slope) angle θ (see Fig. 5).

From Fig. 10 it can be seen that $u_\varphi=\varphi y$ and from (1) $v(L)\equiv u_\theta=2L\theta/3$, where $\theta=Y_{\mathrm{PSD}}/2d$ and $\varphi=X_{\mathrm{PSD}}/2d$. Because $L\gg y$ and experimentally X_{PSD} and Y_{PSD} had the same order of magnitude, $u_\theta \gg u_\varphi$, and therefore $u_s=u_\theta+u_\varphi \cong u_\theta$. Thus, while the Y_{PSD} channel provides direct information on the displacement of the specimen, the X_{PSD} provides complementary information on the applied force, the cantilever dynamic response, and the specimen shear/rotation.

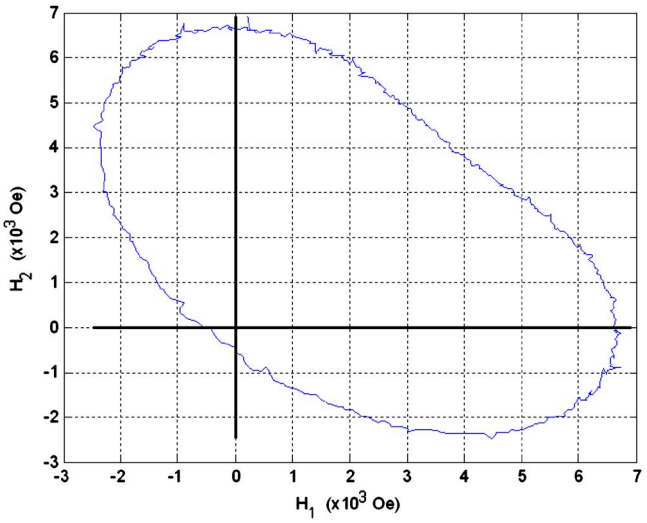

FIG. 11. (Color online) The magnetic field H_2 as a function of the perpendicular magnetic field H_1.

IV. PRELIMINARY RESULTS AND DISCUSSION

The experimental procedure was executed in two steps. The first step was involved characterizing the magnetic driving field. The second step was displacement measurements of the actuator at different mechanical loads up to about 1.5 MPa and magnetic frequency of up to about 70 Hz.

A. Driving magnetic field structure

The driving magnetic field distribution of the AMFG was measured using a Gauss meter (Lakeshore Inc., 475 DSP) in two perpendicular directions in the x-y plane which will be denoted by H_1 and H_2 with a transverse Hall probe (Lakeshore Inc., HMMT-6J08-VR). Field H_1 contracts the crystal (negative strain), while H_2 expands it (positive strain). The magnetic field variation over a cycle is shown in Fig. 11.

B. Actuator displacement measurements and strain calculations

The displacement measurements were performed with different combinations of magnetic field frequencies and mechanical loads. The specimens used had similar dimensions of up to approximately 100 $\mu m\times100$ $\mu m\times5$ mm and the same method of cutting was used for all. Before each experiment, the specimens were cooled under high compressive stress and axial magnetic field to induce a single variant martensitic state. A typical specimen displacement history is depicted in Fig. 12. The driving force for martensitic variant switching is proportional to the difference H_1-H_2, termed the "driving field," which is also plotted in Fig. 11. The fact that the driving field and the displacement are almost exactly in phase indicates the relatively small amount of hysteresis and the potential for high speed actuation using this material.

Focusing on the details of the specimen's actuation pattern, as shown in Fig. 12, we observe small vibration on each cycle. These vibrations were found to be second harmonic oscillations of the cantilever beam and do not affect the results.

V. SUMMARY

The novel system has demonstrated its suitability for testing actuation performances of FSM alloys at small scales.

This article is copyrighted as indicated in the article. Reuse of AIP content is subject to the terms at: http://scitationnew.aip.org/termsconditions. Downloaded to IP: 128.101.142.152 On: Wed, 13 Aug 2014 18:46:48

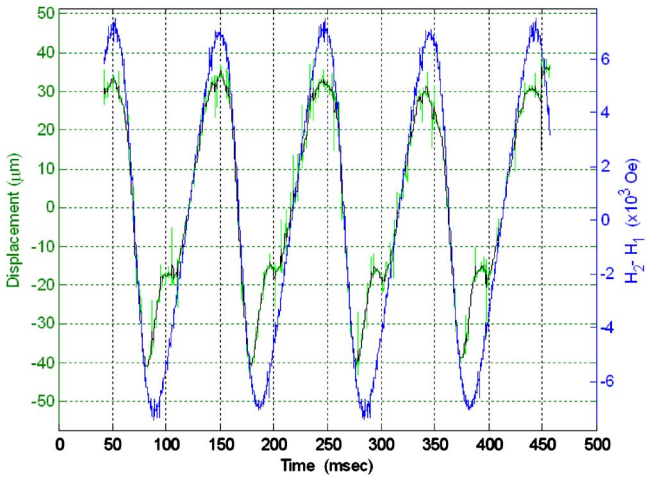

FIG. 12. (Color online) Measured displacement of a 200 μm$\times$200 μm $\times$5 mm specimen and its driving magnetic field with time are shown. The raw displacement data are shown in green, a smoothed displacement is shown in black, and the driving field is in blue.

Preliminary measurements for testing the capabilities of the mechanical apparatus showed that it allows controlling the applied forces with a resolution of micronewton and measuring the displacement with a resolution of 0.1 μm. These capabilities demonstrate the suitability of the system to test microspecimens. The alternating magnetic field generator (AMFG) was proven as a consistent, reliable, and efficient tool for magnetically induced variant switching experiments, and the measured strain is in an overall good agreement with the theoretical constraint model. The results of the measurements demonstrate and verify the high strain capabilities of Ni_2MnGa single crystal, activated by a magnetic field under constant external mechanical loads.

ACKNOWLEDGMENTS

The authors acknowledge the support of ONR N000140610530 (Galfenol MURI), AFOSR STTR FA9550-05-C-0035, and NSF-NIRT DMS-0304326.

[1] R. D. James and M. Wuttig, Philos. Mag. A **77**, 1273 (1998).
[2] K. Ullakko, J. K. Huang, C. Kantner, R. C. O'Handley, and V. V. Kokorin, Appl. Phys. Lett. **69**, 1966 (1996).
[3] R. C. O'Hadley, J. Appl. Phys. **83**, 3263 (1998).
[4] R. Tickle and R. D. James, J. Magn. Magn. Mater. **195**, 627 (1999).
[5] A. Likhachev and K. Ullakko, Phys. Lett. A **275**, 142 (2000).
[6] S. J. Murray, M. Marioni, S. M. Allen, and R. C. O'Handley, Appl. Phys. Lett. **77**, 886 (2000).
[7] A. Sozinov, A. Likhachev, N. Lanska, and K. Ullakko, Appl. Phys. Lett. **80**, 1746 (2002).
[8] E. Clark, in *Ferromagnetic Materials*, edited by E. P. Wohlfarth (North-Holland Publishing, Amsterdam, 1980), Vol. 1, Chap. 7, pp. 531–589.
[9] I. Suorsa, E. Pagounis, and K. Ullakko, J. Magn. Magn. Mater. **272–276**, 2029 (2004).
[10] A. M. Marioni, R. C. O'Handley, and S. M. Allen, Appl. Phys. Lett. **83**, 10 (2003).
[11] R. Tickle, R. D. James, T. Shield, P. Schumacher, M. Wuttig, and V. V. Kokorin, IEEE Trans. Magn. **35**, 4301 (1999).
[12] AdaptaMat Ltd., FSMA actuators (www.adaptamat.com).
[13] Midé Technology Corporation, latching valve system using ferromagnetic shape memory alloy actuators (www.mide.com).
[14] MURI (http://web.mit.edu/bobohand/www/gerver/www/muri/index.html).
[15] K. Bhattacharya, A. Desimone, K. Hane, R. D. James, and C. P. Palmstrom, Mater. Sci. Eng., A **273–275**, 685 (1999).
[16] K. Bhattacharya and R. D. James, J. Mech. Phys. Solids **47**, 531 (1999).
[17] Q. Pan and R. D. James, J. Appl. Phys. **87**, 4702 (2000).
[18] T. W. Shield, Rev. Sci. Instrum. **74**, 4077 (2003).

This article is copyrighted as indicated in the article. Reuse of AIP content is subject to the terms at: http://scitationnew.aip.org/termsconditions. Downloaded to IP: 128.101.142.152 On: Wed, 13 Aug 2014 18:46:48